Electronic Supplementary Information

Peripheral engineering of platinum(II) dicarbene pincer complexes for efficient blue hyperphosphorescent organic light-emitting diodes

Ze-Lin Zhu,[a†*] Yan Jie,[b†] Li-Wen Fu,[c] Chen Cao,[a] Ji-Hua Tan,[a] Sheng-Fu Wang,[c] Yun Chi[ab*] and Chun-Sing Lee[a*]

[a] Center of Super-Diamond and Advanced Films (COSDAF) and Department of Chemistry, City University of Hong Kong, Hong Kong SAR, China, E-mail: zelinzhu-c@my.cityu.edu.hk; apcslee@cityu.edu.hk.

[b] Department of Materials Science and Engineering, City University of Hong Kong, Hong Kong SAR, China, E-mail: yunchi@cityu.edu.hk

[c] Department of Chemistry and Frontier Research Center on Fundamental and Applied Sciences of Matters, Tsing Hua University, Hsinchu 30013, Taiwan, China.

† Equally contributed.

General information:

^{1}H and ^{19}F NMR spectra were measured with Bruker 400MHz AVANCE III instrument or Bruker 600MHz ASCEND AVANCE III HD instrument. Elemental analysis was carried out on a Heraeus CHN-O Rapid Elementary Analyzer. Mass spectra were recorded on HPLC-High Resolution Mass Spectrometer (Sciex X500R Q-TOF). Acetonitrile was use as solvent and a solvent molecule coordinated signal was detected for all measurements (that is target m/z plus 41.0265). Single crystal X-ray diffraction study was measured with a Single Crystal Analyzer (Oxford GEMINI S Ultra) using (Mo-Kα) radiation (λ = 0.71073 Å). Thermogravimetric (TGA) measurements were performed on a Simultaneous Thermal Analyzer (PerkinElmer STA6000) under a nitrogen atmosphere (heating rate:10 °C min^{-1}). UV-Vis spectra were recorded on a HITACHI U-3900 spectrophotometer. The steady-state emission spectra and lifetime studies were measured with an Edinburgh FL 980 photon-counting system. To determine the photoluminescence quantum yield (Φ) in solution, samples were degassed using at least three freeze-pump-thaw cycles. Spectral grade solvents (Merck) were used as received. Cyclic voltammetry was conducted on a CHI621A Electrochemical Analyzer equipped with a three-electrode system (glassy carbon: working electrode, platinum wire: auxiliary electrode, Ag/AgCl: reference electrode). N_2 saturated acetonitrile with 0.1 M NBu_4PF_6 supporting electrolyte was used as solvent and potentials were referenced externally to the ferrocenium/ferrocene (Fc^+/Fc) couple. All calculations were performed with the Gaussian 16 program package. The electron excitation analysis was finished by using the Multiwfn 3.7.[1]

Device fabrication and measurement:

Before device fabrication, pre-cleaned ITO-coated glass substrates with a sheet resistance of 15 Ω $square^{-1}$ were subjected to UV-ozone treatment for 20 min. All the materials are purchased from Lumtec (Taiwan) and organic films were deposited at a rate of 0.5–1.0 Å s^{-1} by thermal evaporation in a deposition chamber with a base vacuum of 1 × 10^{-6} Torr. Current density–voltage (*J-V*) characteristics were recorded on a Keithley 237 power source (Tektronix). Luminance and electroluminescence spectra were measured by a PMA-12 photonic multichannel analyzer (Hamamatsu). Except the Pt(II) chlorides, all materials used to fabricated device were purchased from PURI Materials and Lumtec Corp. All measurements were performed in ambient without encapsulation.

Förster energy transfer radius calculation:

The FET radii (R_F) was calculated by below equation.[2,3]

$$J = \int \varepsilon_A(\lambda) F_D(\lambda) \lambda^4 d\lambda \quad \text{----------(1)}$$

$$R_0^6 = \Phi_D \cdot \kappa^2 \left(\frac{9000.\ ln10}{128.\ \pi^5.\ N_A.\ n^4} \right) . \int_0^\infty \varepsilon_A(\lambda) F_D(\lambda) \lambda^4 d\lambda \quad \text{----------(2)}$$

The specific FET radii (R_{0S}) were calculated by the above equation, in which Φ_D is the photoluminescence quantum efficiency of donor; κ^2 is the configurational factor between the energy donor and energy acceptor (assumed to be 2/3 with regard of random distribution); N_A is the Avogadro's constant; n is the refractive index of the medium and $F_D(\lambda)$ is the emission spectra of donor with normalized area; $\varepsilon_A(\lambda)$ is the molar absorption coefficient (mol m^{-4}).

Table S1 Calculated transition energy (λ), main orbital contributions to the lowest singlet and triplet excited states and transition character assignment of Pt(II) complexes.

complexes	**state**	**λ (nm)**	**Orbital contribution (> 10%)**	**Assignment**
MeCF3Pt	S_0-S_1	352.23	HOMO-1 → LUMO (98.3%)	MLCT/ILCT/XLCT
	S_0-T_1	427.38	HOMO → LUMO (81.1%)	MLCT (12.9%)/ILCT/XLCT (29.2%)
IPrCF3Pt	S_0-S_1	350.21	HOMO-1 → LUMO (98.2%)	MLCT/ILCT/XLCT
	S_0-T_1	426.03	HOMO → LUMO (80.6%)	MLCT (11.5%)/ILCT/XLCT (26.2%)
IPrtBuPt	S_0-S_1	349.91	HOMO → LUMO (95.5%)	MLCT/ILCT/XLCT
	S_0-T_1	427.05	HOMO → LUMO (80.9%)	MLCT (11.8%)/ILCT/XLCT (20.5%)

Table S2 Selected bond angles and bond lengths.

compound	**Pt-C_{Ar} [Å]**	**Pt-C_{NHC} [Å]**	**Pt-Cl [Å]**	**C_{NHC}-Pt-C_{NHC} [°]**	**C_{Ar}-Pt-Cl [°]**
MeCF3Pt	1.935	2.025/2.024	2.412	157.29	179.68
IPrCF3Pt	1.948	2.027/2.033	2.381	158.29	177.59
IPrtBuPt	1.938	2.032/2.040	2.399	156.77	178.23

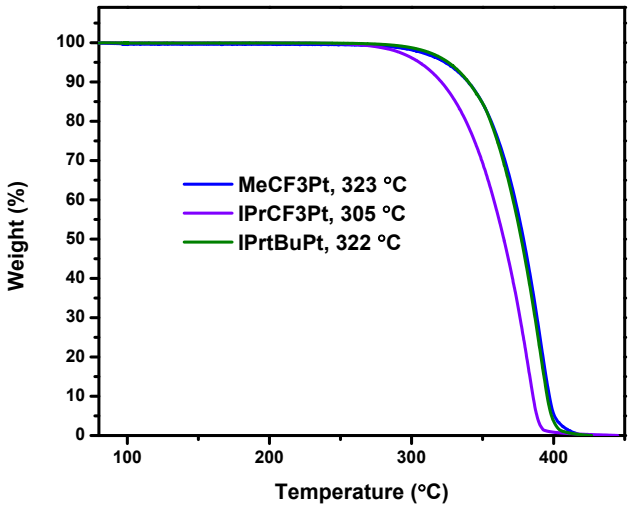

Fig. S1. TGA curves of studied compounds measured under N_2 atmosphere.

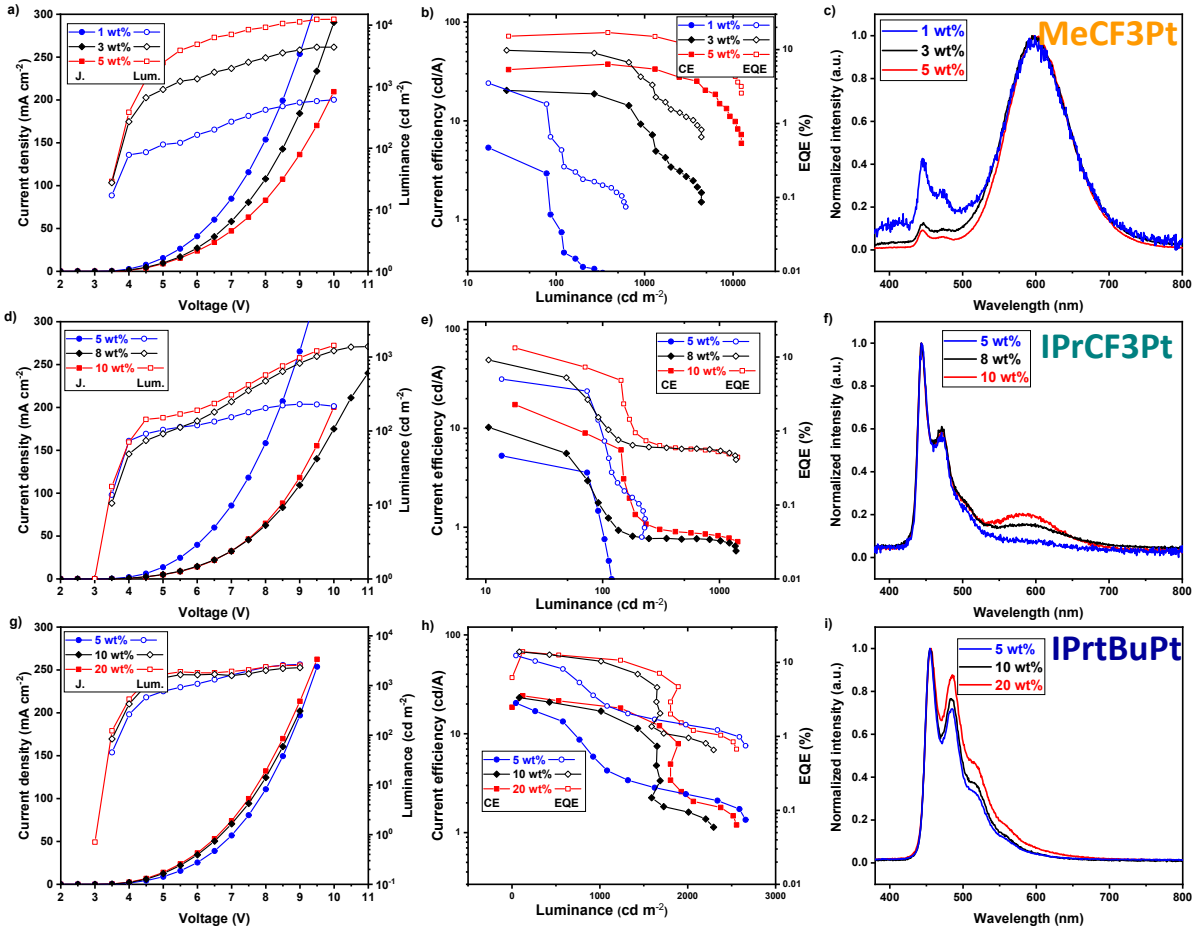

Fig. S2 a), d) and g) current density–voltage–luminance plots; b), e) and h) current efficiency–luminance–EQE curses and c), f) and i) EL spectrum of MeCF3Pt (top row), IPrCF3Pt (middle row) and IPrtBuPt (bottom row) OLED.

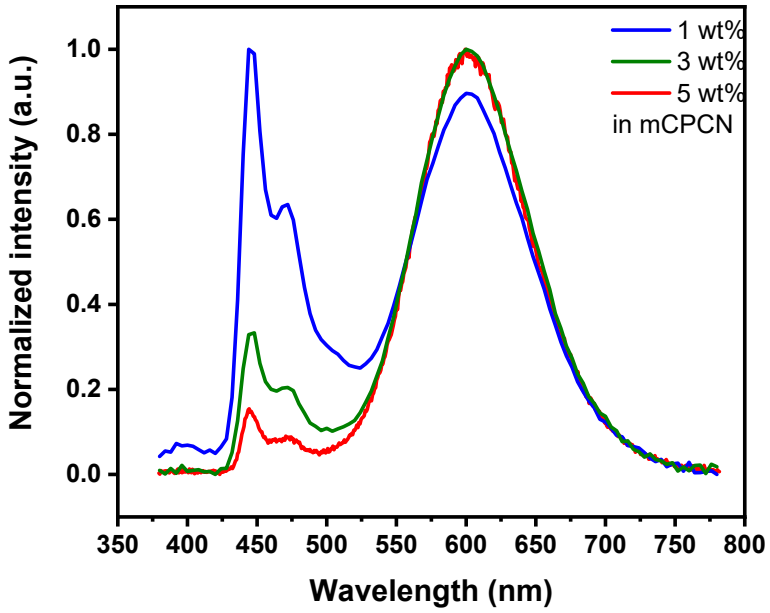

Fig. S3 Concentration dependent PL spectrum of MeCF3Pt.

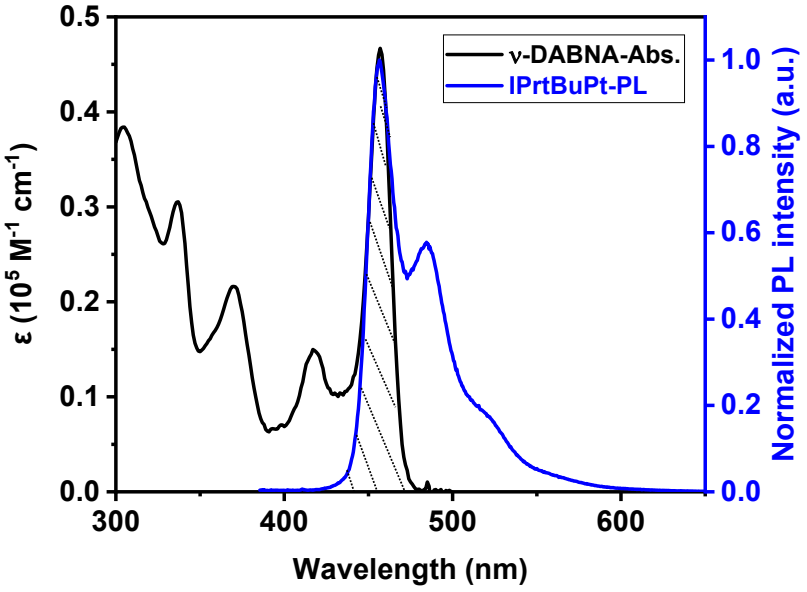

Fig. S4 Overlap area between UV-Vis absorption spectrum of *ν*-DABNA and PL spectrum of IPrtBuPt.

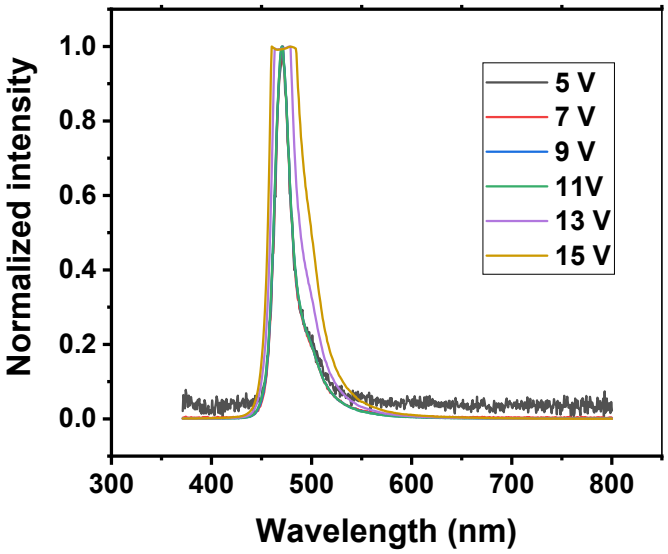

Fig. S5 Voltage-dependent EL spectra of IPrtBuPt-based hyper-OLED.

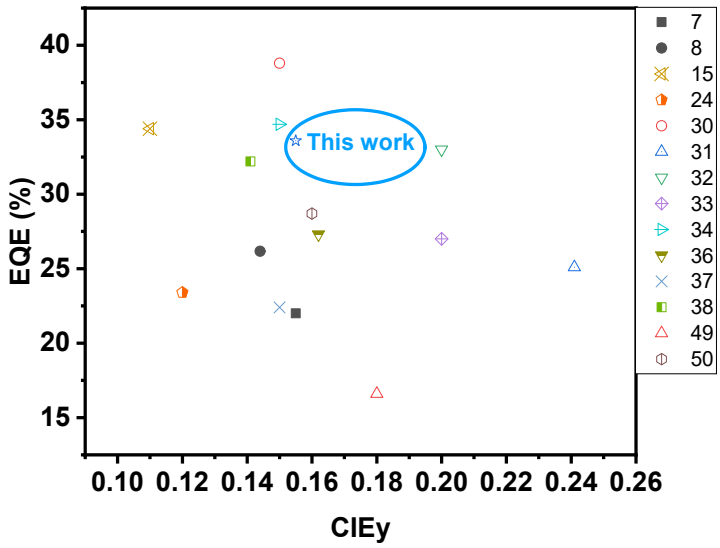

Fig. S6 Comparing performances of representative hyper-OLEDs based on *ν*-DABNA (No. in legend corresponding to ref. No. in the main text).

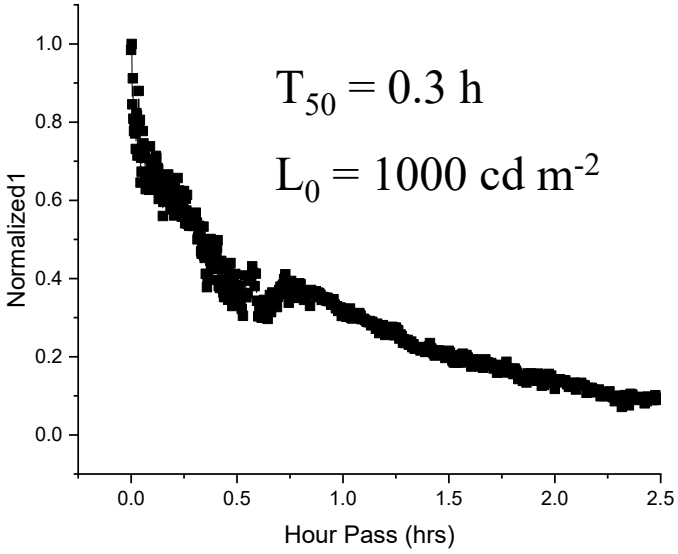

Fig. S7 Device lifetime of IPrtBuPt-based hyper-OLED.

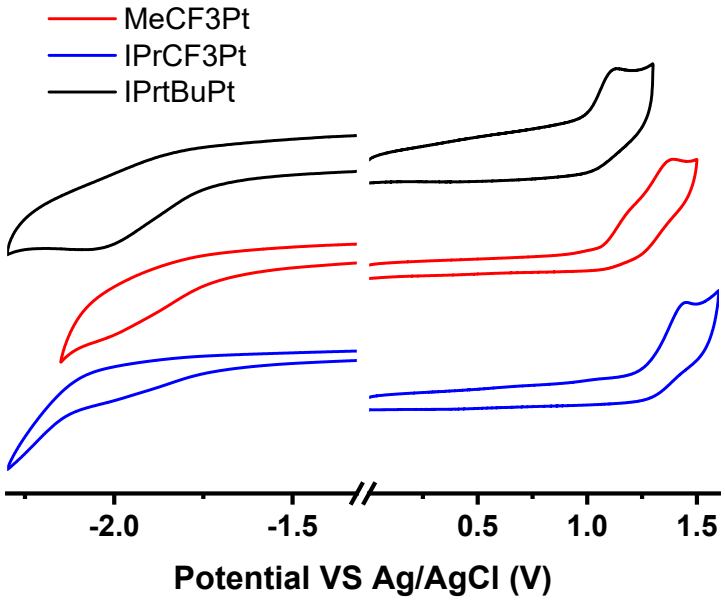

Fig. S8 Cyclic voltammetry study of MeCF3Pt, IPrCF3Pt and IPrtBuPt.

Table S3 Crystal data and structure refinement for MeCF3Pt.

Empirical formula	$C_{15.33}H_{12.67}Cl_{1.67}F_3N_4Pt$
Formula weight	564.13
Temperature/K	173(2)
Crystal system	monoclinic
Space group	$P2_1/c$
a/Å	22.9117(7)
b/Å	10.5094(3)
c/Å	23.4650(6)
α/°	90
β/°	118.9560(10)
γ/°	90
Volume/Å^3	4943.8(2)
Z	12
ρ_{calc}g/cm^3	2.274
μ/mm^{-1}	8.823
F(000)	3192.0
Crystal size/mm^3	0.51 × 0.25 × 0.03
Radiation	MoKα (λ = 0.71073)
2Θ range for data collection/°	4.376 to 52.788
Index ranges	$-28 \leq h \leq 28$, $-12 \leq k \leq 13$, $-29 \leq l \leq 29$
Reflections collected	43144
Independent reflections	10105 [R_{int} = 0.0374, R_{sigma} = 0.0335]
Data/restraints/parameters	10105/70/709
Goodness-of-fit on F^2	1.021
Final R indexes [I>=2σ (I)]	R_1 = 0.0249, wR_2 = 0.0579
Final R indexes [all data]	R_1 = 0.0304, wR_2 = 0.0603
Largest diff. peak/hole / e Å^{-3}	0.96/-1.59

Table S4 Crystal data and structure refinement for IPrCF3Pt.

Empirical formula	$C_{19}H_{20}ClF_3N_4Pt$
Formula weight	591.93
Temperature/K	173(2)
Crystal system	orthorhombic
Space group	Pbca
a/Å	12.3204(3)
b/Å	16.7473(3)
c/Å	39.9010(9)
α/°	90
β/°	90
γ/°	90
Volume/Å^3	8232.9(3)
Z	16
ρ_{calc}g/cm^3	1.910

μ/mm^{-1}	6.985
F(000)	4544.0
Crystal size/mm^3	0.47 × 0.21 × 0.03
Radiation	MoKα (λ = 0.71073)
2Θ range for data collection/°	4.584 to 52.764
Index ranges	-13 ≤ h ≤ 15, -20 ≤ k ≤ 20, -49 ≤ l ≤ 49
Reflections collected	39834
Independent reflections	8242 [R_{int} = 0.0495, R_{sigma} = 0.0423]
Data/restraints/parameters	8242/777/621
Goodness-of-fit on F^2	1.064
Final R indexes [I>=2σ (I)]	R_1 = 0.0463, wR_2 = 0.1392
Final R indexes [all data]	R_1 = 0.0648, wR_2 = 0.1516
Largest diff. peak/hole / e Å^{-3}	2.12/-1.94

Table S5 Crystal data and structure refinement for IPrtBuPt.

Empirical formula	$C_{22}H_{29}ClN_4Pt$
Formula weight	580.03
Temperature/K	213(2)
Crystal system	monoclinic
Space group	$P2_1/c$
a/Å	10.8304(3)
b/Å	25.8800(7)
c/Å	17.1779(4)
α/°	90
β/°	103.0080(10)
γ/°	90
Volume/Å^3	4691.3(2)
Z	8
ρ_{calc}g/cm^3	1.642
μ/mm^{-1}	6.110
F(000)	2272.0
Crystal size/mm^3	0.25 × 0.11 × 0.03
Radiation	MoKα (λ = 0.71073)
2Θ range for data collection/°	4.366 to 52.786
Index ranges	-13 ≤ h ≤ 13, -32 ≤ k ≤ 32, -19 ≤ l ≤ 21
Reflections collected	30971
Independent reflections	9530 [R_{int} = 0.0584, R_{sigma} = 0.0644]
Data/restraints/parameters	9530/294/578
Goodness-of-fit on F^2	1.003
Final R indexes [I>=2σ (I)]	R_1 = 0.0390, wR_2 = 0.0721
Final R indexes [all data]	R_1 = 0.0689, wR_2 = 0.0843
Largest diff. peak/hole / e Å^{-3}	0.82/-1.07

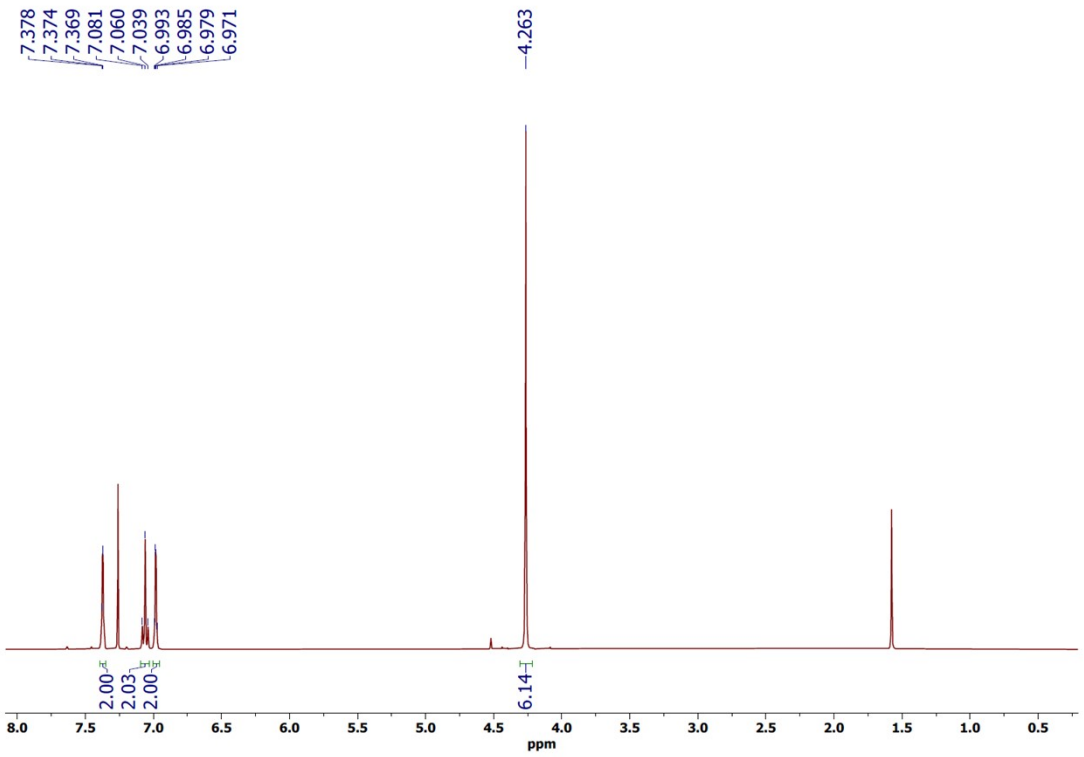

Fig. S9. ^{1}H-NMR (400 MHz) spectrum of MeCF3Pt.

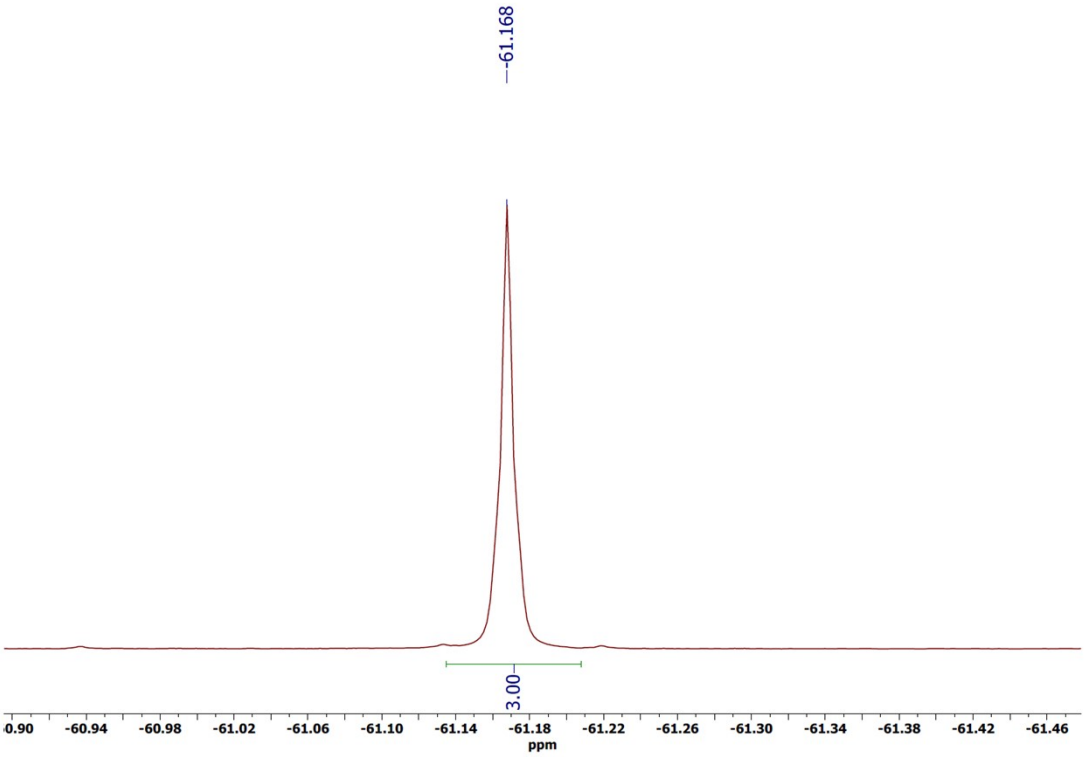

Fig. S10. ^{19}F-NMR (376 MHz) spectrum of MeCF3Pt.

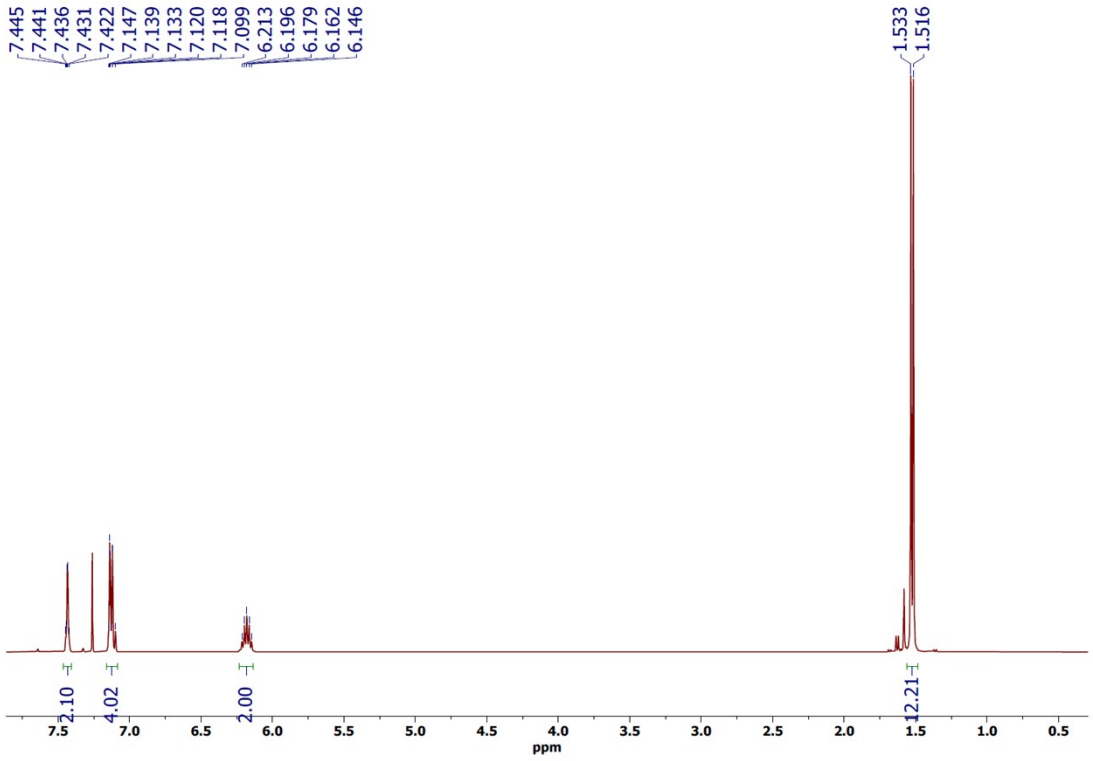

Fig. S11. [1]H-NMR (400 MHz) spectrum of IPrCF3Pt.

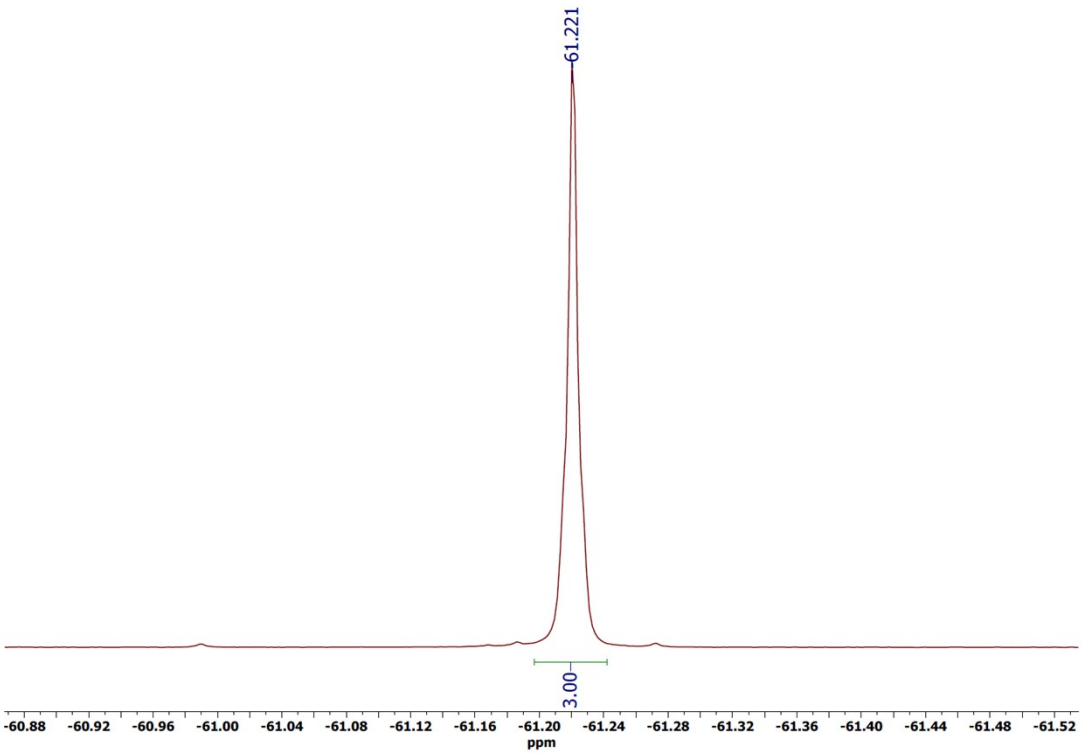

Fig. S12. [19]F-NMR (376 MHz) spectrum of IPrCF3Pt.

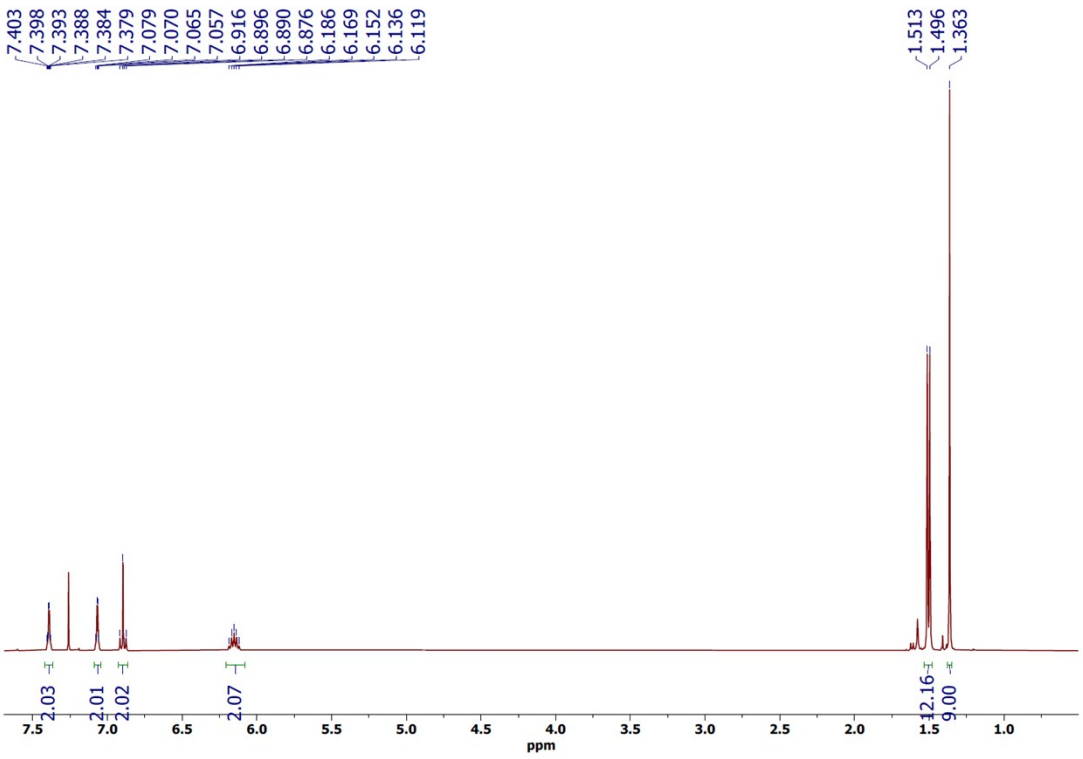

Fig. S13. ^{1}H-NMR (400 MHz) spectrum of IPrtBuPt.

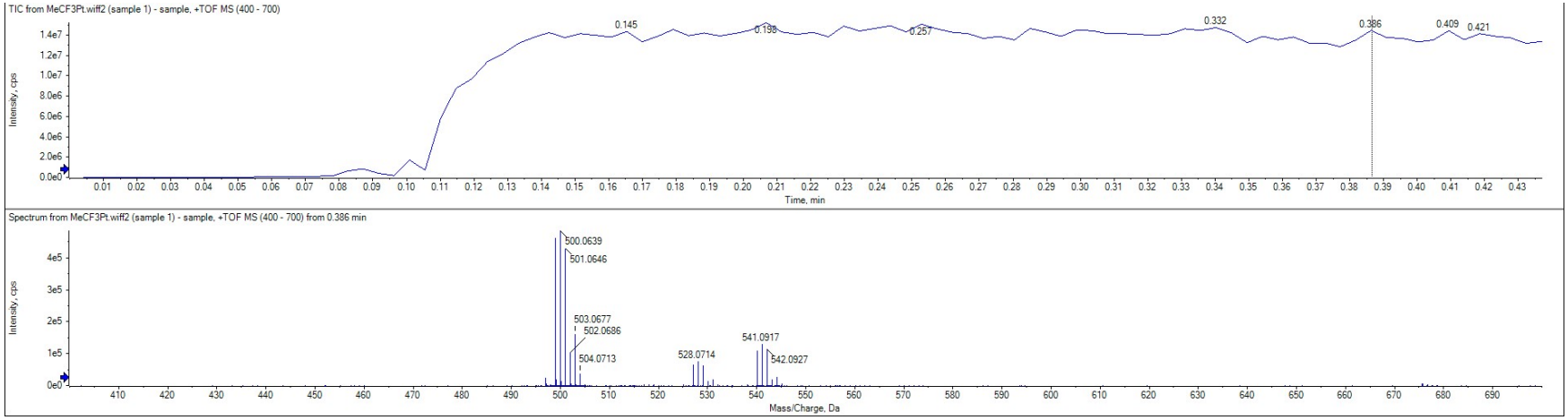

Fig. S14. HR-MS spectrum of **MeCF3Pt**.

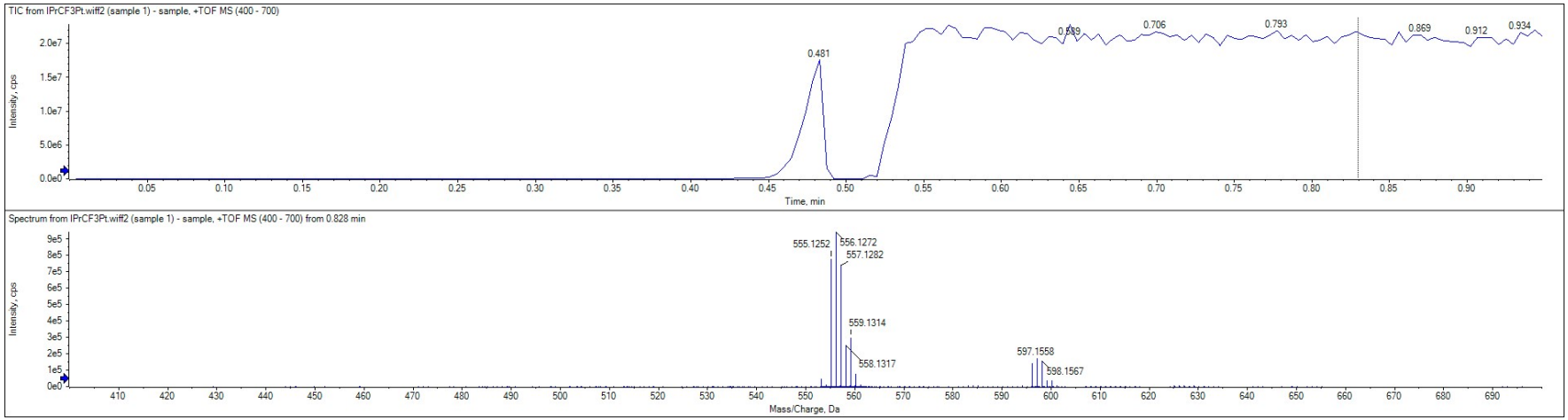

Fig. S15. HR-MS spectrum of **IPrCF3Pt**.

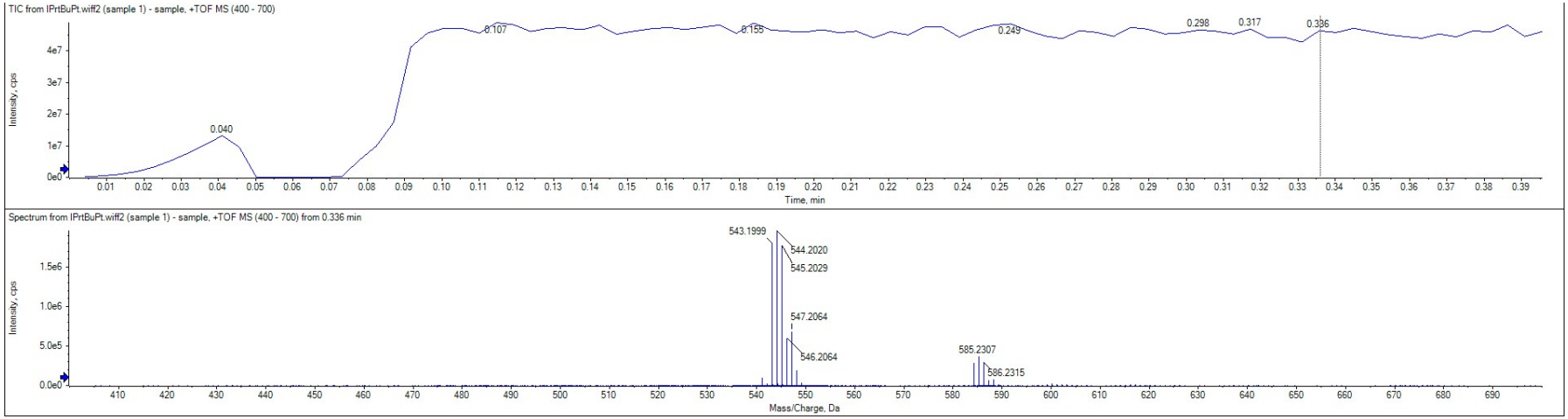

Fig. S16. HR-MS spectrum of **IPrtBuPt**.

References

1 T. Lu and F. Chen, Multiwfn: A multifunctional wavefunction analyzer, *J. Comput. Chem.*, 2012, **33**, 580.

2 N. Hildebrandt and I. L. Medintz, FRET-Forster Resonance Energy Transfer: From Theory to Applications, Wiley-VCH Verlag GmbH, 2014.

3 C. Zhang, Y. Lu, Z. Liu, Y. Zhang, X. Wang, D. Zhang and L. Duan, A π–D and π–A Exciplex-Forming Host for High-Efficiency and Long-Lifetime Single-Emissive-Layer Fluorescent White Organic Light-Emitting Diodes, *Adv. Mater.*, 2020, **32**, 2004040.